

Photothermoelectric Response of $\text{Ti}_3\text{C}_2\text{T}_x$ MXene Confined Ion Channels

Seunghyun Hong, Guodong Zou, Hyunho Kim, Dazhen Huang, Peng Wang,* and Husam N. Alshareef*



Cite This: *ACS Nano* 2020, 14, 9042–9049



Read Online

ACCESS |



Metrics & More



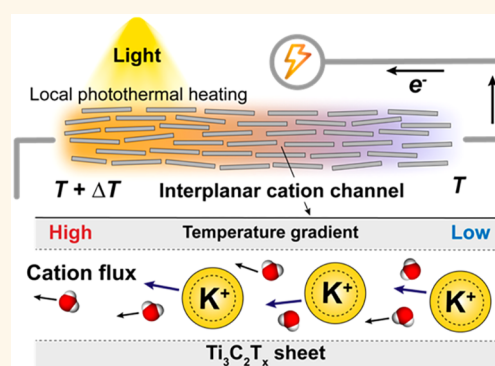
Article Recommendations



Supporting Information

ABSTRACT: With recent growing interest in biomimetic smart nanochannels, a biological sensory transduction in response to external stimuli has been of particular interest in the development of biomimetic nanofluidic systems. Here we demonstrate the MXene-based subnanometer ion channels that convert external temperature changes to electric signals *via* preferential diffusion of cations under a thermal gradient. In particular, coupled with a photothermal conversion feature of MXenes, an array of the nanoconfined $\text{Ti}_3\text{C}_2\text{T}_x$ ion channels can capture trans-nanochannel diffusion potentials under a light-driven axial temperature gradient. The nonisothermal open-circuit potential across channels is enhanced with increasing cationic permselectivity of confined channels, associated with the ionic concentration or pH of permeant fluids. The photothermoelectric ionic response (evaluated from the ionic Seebeck coefficient) reached up to $1 \text{ mV}\cdot\text{K}^{-1}$, which is comparable to biological thermosensory channels, and demonstrated stability and reproducibility in the absence and presence of an ionic concentration gradient. With advantages of physicochemical tunability and easy fabrication process, the lamellar ion conductors may be an important nanofluidic thermosensation platform possibly for biomimetic sensory systems.

KEYWORDS: titanium carbide, MXene lamellar membranes, nanoconfined cation channels, photothermal conversion, thermo-osmosis, thermoelectric Seebeck coefficient



With recent advances in nanofabrication technologies and growing interest in bioinspired smart nanochannels, significant progress has been made in the design and fabrication of artificial nanofluidic channels, mimicking tailored functions of biological ion channels.^{1,2} For instance, human skin, possessing various sensory receptors, has inspired extensive research to develop nanofluidic sensory systems having a fast and selective response to different chemical and physical stimuli. Among various types of biological ion channels, thermosensitive transient receptor potential (thermoTRP) cation channels have been of key interest in such nanofluidic applications as bionic thermometer and thermal energy conversion and harvesting.^{3,4} The thermoTRP channels in the thermoreceptor cells of the skin convert external thermal stimuli into electrical signals associated with action potentials.

In earlier studies, temperature-sensitive gatekeepers such as elastin-like polypeptide loops or polyNIPAM brushes, which were grafted onto synthetic or protein pores, described crucial roles in controlling the ionic flow in response to temperature changes.^{5–10} Most recently, intrinsic nanochannels with ultraconfined pores and plenty of surface charges revealed their potential applications to a variety of external stimuli-

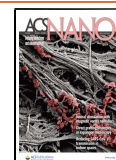
responsive ionic sensory systems.^{11–14} When the confined space of nanochannels is as small as the Debye screening length near charged walls, an overlapped electrical double layer (EDL) mostly composed of surface charge-compensating counterions can be created inside nanoconfined channels, which enables charge-selective ion transportation in response to external stimuli.^{14–17} Especially, under chemical potential driven by temperature or salinity, such charge-selective ion transportation can serve as a driving force to generate electrical potential. In light of this feature, stimuli-responsive artificial nanochannels with surface charges have been explored with a wide range of fluidic conduits such as perforated nanopores, nanoslits, or nacre-inspired lamellae nanochannels.^{14,18–21}

Focusing on nanoporous lamellae structures composed by multilayered two-dimensional (2D) nanosheets, we explored the cation channels of metal carbide and nitride (MXene)

Received: May 16, 2020

Accepted: June 15, 2020

Published: June 15, 2020



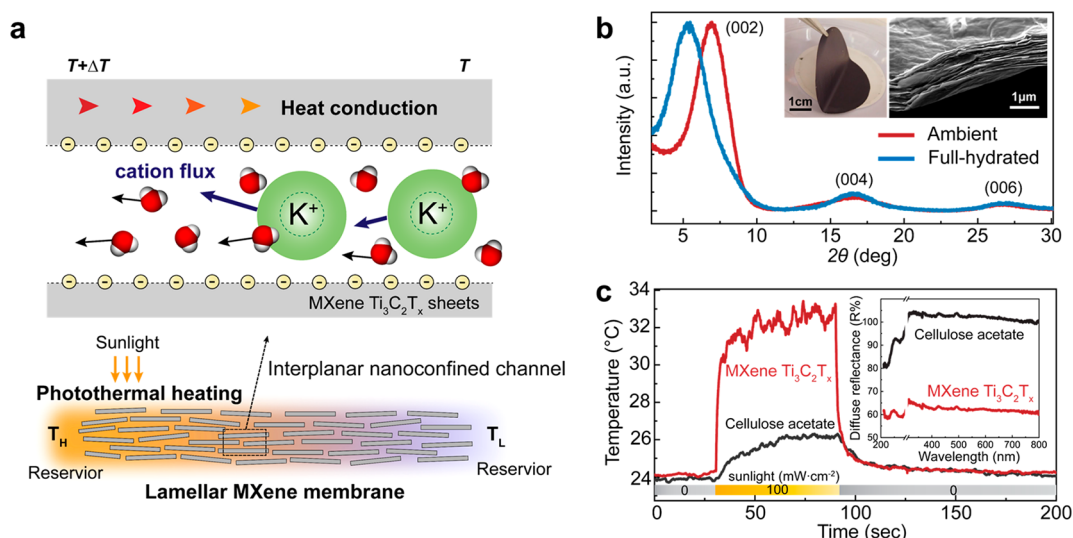


Figure 1. Photothermally responsive ion channels. (a) Generation of transverse photothermoelectric voltages across lamellar $Ti_3C_2T_x$ membranes under light illumination. Under a light-driven temperature gradient, the hydrated cations and water molecules display a directional thermo-osmotic transport from cold to hot sides. (b) X-ray diffraction of the lamellar $Ti_3C_2T_x$ membranes with highly aligned interplanar spacing. Inset illustrates, respectively, an optical image of the MXene membrane and a SEM image of its cross-sectional area. (c) Photothermal conversion of the MXene membranes under light illumination. Supplied light energy onto the MXene membranes is approximately 8 mW. Inset shows a diffuse reflectance of dried MXene and cellulose acetate films, respectively.

lamellar membranes in pursuit of mimicking thermosensing process of thermoTRP channels. As the lamellar membranes provide densely interconnected and interplanar nanocapillaries with subnanometer dimensions, it is beneficial to detect collective motion of ions in response to electrochemical potential. Additionally, the nanoconfined channels are covered by an EDL, enabling charge-permeable transport. Arising from aqueous etching and exfoliation processes during MXene synthesis, negatively charged surface terminal groups ($-O$, $-OH$, or $-F$) on the MXene sheets contribute to creating subnanometer-sized interplanar spacing in the lamellar membranes and endows the MXene channels with the surface charges.^{14,22,23} The MXene-based lamellar membrane makes an enticing ion-selective conductor with potential applications in salinity-gradient energy harvesting and ion-sieving membranes for water purification.^{14,24–26}

In this study, we investigated ionic thermoelectric transport through $Ti_3C_2T_x$ MXene-based fluidic channels, especially under a temperature gradient created by light-driven heating. Coupled with inherent photothermal conversion performance of MXene materials,^{23,27,28} the subnanometer capillaries in MXene membranes exhibit thermo-osmotic cation flow and consequential thermoelectric response of up to $1.0 \text{ mV}\cdot\text{K}^{-1}$ under local sunlight exposure. Even under tiny temperature differences below 1 K, the MXene channels had a very sensitive thermoelectric response. Such nonisothermal voltage is found to be enhanced with increasing cationic permselectivity of channels, which is associated with ionic concentration or pH of permeant fluids. Furthermore, the MXene ion channels revealed stable and reproducible responses to temperature change under light illumination. We envision the MXene cation channels mimicking the biological thermosensation process would offer a promising avenue for many potential applications, including temperature sensing, photodetection, or photothermoelectric energy harvesting.

RESULTS AND DISCUSSION

Figure 1a demonstrates the ionic thermoelectric voltage generation through the confined ion channels under a local light irradiation-driven temperature gradient. Transverse fluidic channels in the lamellar MXene membranes offer the cation-exchange features enabled by EDL inside the nanoconfined channels. When the channel height is comparable to the electrostatic screening length given by the Debye length, the EDL formed on each interplane can overlap, enabling the strong cation-selective passage under chemical potentials.^{14–17} When the fluidic channel is stimulated by localized thermal excitation, a temperature gradient can be created through the permeating fluids. Note that a chemical potential of water decreases linearly with the increase of temperature, and water molecules are prone to moving from higher chemical potential to lower chemical potential. As a consequence of local photothermal heating, a chemical potential along the temperature gradient can create a thermo-osmotic ion transport with concurrent water flux from cold to hot sides.^{11,29} In principle, a transport takes place in a direction producing more entropy, and more specifically heat diffuses down, whereas a confined permeant flows against a thermal gradient.²⁶ Aiming to create such thermodynamic conditions under light illumination, the MXene lamellar structures are exploited, offering outstanding photothermal conversion performance as well as plenty of surface charge groups accommodating hydrated cations.

The $Ti_3C_2T_x$ MXene sheets were prepared from MAX phase (Ti_3AlC_2) through selective etching of Al using a mixture of aqueous hydrochloric acid and lithium fluoride (Experimental Section and Figure S1). The scanning electron microscopy (SEM) image of synthesized MXene monolayers clearly verifies the presence of planar surfaces with sharp and well-defined edges. Atomic force microscopic measurement shows that a monolayer $Ti_3C_2T_x$ possesses a thickness of 1.5 to 2.0 nm while further confirming its well-defined planar morphology. The observed larger thickness, taking into account a theoretical monolayer thickness of around 0.98 nm,^{30,31} is

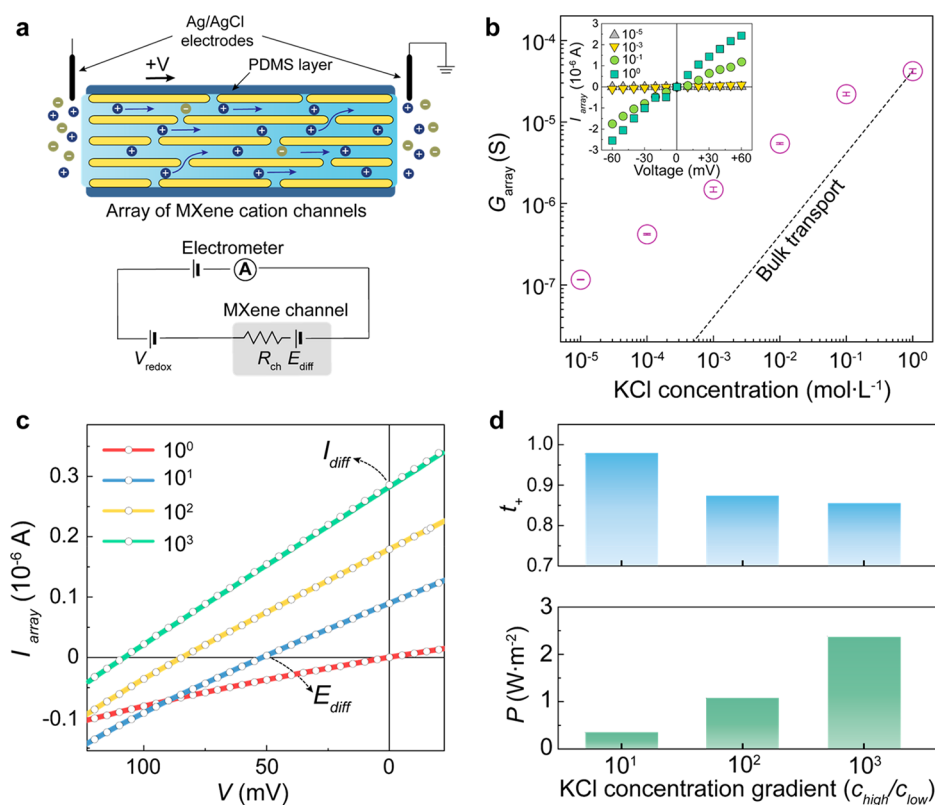


Figure 2. Cation-selective ion transport. (a) Schematic of the experimental setup. A PDMS-encapsulated MXene lamellar membrane offers an array of MXene cation channels while avoiding possible thermal evaporation effects. An equivalent circuit diagram is displayed in the inset. (b) Surface-charge-governed ion transport. Inset shows the IV curves at varying potassium chloride concentrations. (c) IV curves under a salinity concentration gradient at neutral pH. (d) Cation transference number and maximum osmotic power density through the MXene channels, evaluated with the open-circuit voltage and short-circuit current under different salt concentration gradients.

most likely associated with the absorbed water or impurities on the $\text{Ti}_3\text{C}_2\text{T}_x$ sheets. The lamellar MXene membranes were fabricated by a vacuum-filtration method of aqueous-exfoliated $\text{Ti}_3\text{C}_2\text{T}_x$ sheets with porous polymeric supports.^{32–34} The lamellar structure of the MXene membrane was confirmed from a cross-section areal SEM image as shown in the inset of Figure 1b.

As a prerequisite for the ion-selective passage, the nanoconfined interplanar channel present in lamellar MXene membranes was verified by the X-ray diffraction (XRD) analysis of fully hydrated $\text{Ti}_3\text{C}_2\text{T}_x$ lamellar membranes. The interlayer spacing is calculated using Bragg's law, $\lambda = 2d \sin \theta$, where λ is the wavelength of X-ray radiation, d is the d -spacing, and θ is the diffraction angle. As shown in Figure 1b, the diffraction peak (002) at around 5.28° for the fully hydrated membrane indicates a d -spacing of around 1.67 nm, which is larger by around 0.4 nm than that of the ambient-state membrane. This volumetric expansion in hydration is strongly correlated with water molecules accumulated in the lamellae channels possessing abundant surface charge groups.^{22–26} The effective interplanar height for the fluidic motions is estimated to be around 0.69 nm, which is large enough for hydrated small ions such as K^+ or Na^+ to pass through.^{15,35,36} Moreover, high optical absorptivity of the MXene membranes, essential for photothermal heating, was verified from their rapid temperature changes under light, which is further supported by the lower diffuse reflectance of $\text{Ti}_3\text{C}_2\text{T}_x$ films compared to that of cellulose acetate (Figure 1c). Given that the darkening effect works in the wet state, attributable to the significant decrease

of light scattering from liquid to the material interface, the diffuse reflectance of wet MXene membranes can be further reduced.³⁷

To elucidate the charge-selective ion transport through MXene nanoconfined channels, the transverse ion flux was measured at different equimolar concentrations as well as salt concentration gradients (Figure 2a). The width, height, and length of the singular two-dimensional channel are approximately 3 mm, 0.69 nm, and 10 mm, respectively. Based on the identified interplanar spacing from XRD analysis, the effective transport area is estimated to be $3.27 \times 10^{-9} \text{ m}^2$ with a porosity of around 41.7% for a 2 μm thick membrane (see Supporting Information for details). Unless otherwise mentioned, all the ion transport measurements were conducted at a membrane thickness of 2 μm . Figure 2b shows the ionic channel conductances (G_{array}) of the membranes at varying concentrations, and the deviated transport from bulk transport below KCl 1 $\text{mol}\cdot\text{L}^{-1}$ confirms the dominant surface charge effect at lower salt concentration.^{14–16} Furthermore, a scaling behavior is observed at low salt concentration, which is caused by salt-concentration-dependent variation of surface charges as previously reported.^{38,39} The current–voltage (IV) transport was also investigated under a salt concentration gradient ($c_{\text{high}}/c_{\text{low}}$) of 1 to 10^3 at a fixed c_{low} of $10^{-4} \text{ mol}\cdot\text{L}^{-1}$ (Figure 2c). A direction of short-circuit current (I_{diff}) in the absence of bias is consistent with a net flow of positive charges, and this charge-selective osmotic flow produces an open-circuit voltage (E_{diff}) across the membranes. Salt bridge Ag/AgCl electrodes were used for precise measurement of the open-circuit voltage.¹⁹

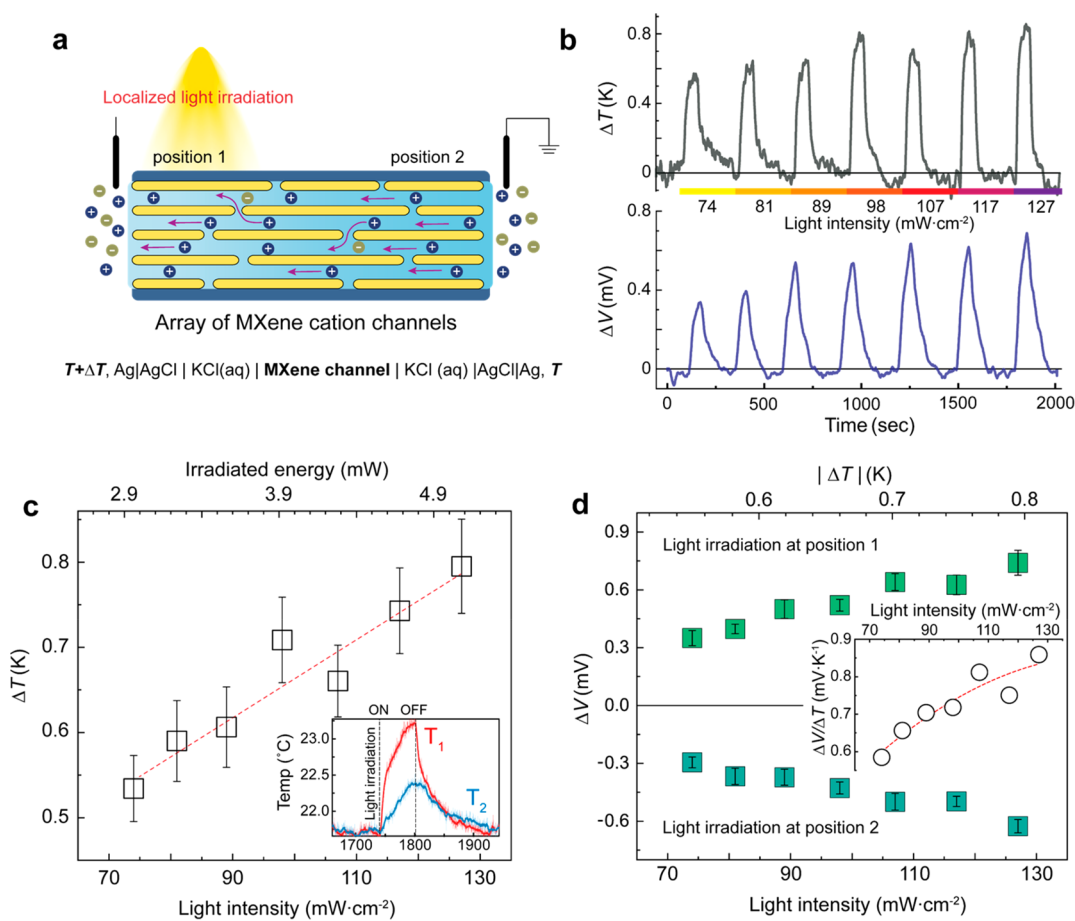


Figure 3. Light-controlled photothermal ionic responses. (a) Schematic of the experimental setup. The MXene cation channels exhibit the thermo-osmotic ionic flow directing from unilluminated to illuminated sides. The temperature profile is measured using a thermographic camera at each designated position, and the electrical potentials using the electrometer. (b) Time-dependent temperature gradient and photothermal voltages when irradiated at position 1. The light is irradiated for 60 s at each light intensity. (c) Proportional increment of temperature gradient at elevated light intensity. Inset shows time-dependent temperature changes at positions 1 and 2, respectively, under light illumination of 127 $\text{mW}\cdot\text{cm}^{-2}$. (d) Photothermal voltages under elevated light intensity at different irradiation positions. Inset displays the calculated ionic Seebeck coefficient from the photothermal voltages, independently of the irradiation positions.

With an increasing salt concentration gradient, the IV curves show obvious increment in both I_{diff} and E_{diff} . For a quantitative evaluation on the charge selectivity, a cation transference number (t_+) is calculated by the equation $t_+ = 0.5(1 + E_{\text{diff}}/E_{\text{redox}})$, where E_{redox} is a redox potential arising from the unequal chloride concentration at the two Ag/AgCl electrodes.^{15,21,40} For the redox potentials, theoretically predicted values were applied over varying salt concentration gradients of 10^1 to 10^3 .^{15,21} As shown in Figure 2d, it approaches 0.97 under a 10-fold difference in salt concentration, close to unity cation selectivity. Note that the transference number is defined as the fraction of the current carried by either the anion or the cation to the total electric current.^{15,40} A higher transference number under a 10-fold difference is attributed to stronger cationic selectivity observed in the lower concentration regime. This feature is previously reported from graphene oxide lamellar membranes as well.¹⁵ The salinity gradient-induced osmotic power further supports their charge-selective ion transport through the confined channels with negative surface charges.⁴⁰

To introduce a thermochemical potential across the fluidic MXene channels, localized photothermal heating was applied, creating an axial temperature gradient (Figure 3a). The array of transverse ion channels generates a parallel flux of electrical

double layers under thermal potential, and their directionality is strongly associated with the light irradiation position. The ionic thermoelectric response under light is characterized with the ionic Seebeck coefficient calculated from an open-circuit voltage through ionic channels by a given temperature difference.⁴¹ The employed polydimethylsiloxane (PDMS) layers exhibiting excellent optical transparency and thermal insulation are beneficial for suppressing the optical scattering or thermal dissipation under light illumination. Particularly, due to the encapsulated structure by PDMS, interfacial factors influencing the thermoelectric response could be ruled out, such as thermal evaporative cooling and derived fluidic motion under light.^{27,42,43}

At a light intensity spanning a range of 74 to 127 $\text{mW}\cdot\text{cm}^{-2}$, the temperature gradient and derived photothermal voltages were investigated across the MXene channels. The KCl concentration is fixed to $5 \times 10^{-4} \text{ mol}\cdot\text{L}^{-1}$. With increasing the light intensity, a proportional open-circuit voltage (ΔV) is observed across the produced temperature gradient, yielding a positive ionic Seebeck coefficient (Figure 3b). The thermo-osmotic ionic flow directing unilluminated to illuminated sides determines the magnitude and polarity of the generated open-circuit voltages. In addition, the MXene channels exhibited a prompt response under light stimulation (Figure S3). The

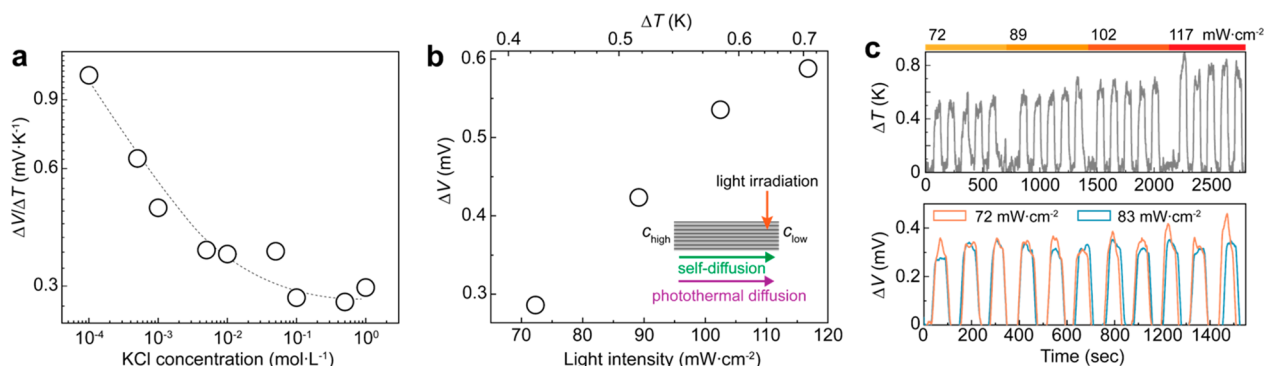


Figure 4. Electrolyte-controlled photothermal ionic responses. (a) KCl concentration-dependent photothermoelectric response. (b, c) Photothermoelectric response and its cyclic stability under a KCl concentration gradient of a c_{high} of $0.5 \text{ mol}\cdot\text{L}^{-1}$ to a c_{low} of $10^{-2} \text{ mol}\cdot\text{L}^{-1}$.

rapid photothermal heating of nanoconfined fluids may be responsible for the instantaneous thermo-osmotic motion. The temperature gradient (ΔT) between designated positions as 1 and 2 increases proportionally to the energy of irradiated light, irrespective of the light irradiation position (Figure 3c). When the MXene channel is locally irradiated, a stable thermal flux across the channel could be identified over varying light intensities. We ascribe this conductive thermal feature to drive the stable temperature difference across the interlayer water in the transverse cation channels.

As shown in Figure 3d, the MXene nanochannels obviously illustrate a proportionate rise in the ionic thermoelectric voltages under elevated light intensity. The channels also produced the different polarity of the thermal voltages, depending on the irradiation position. A prolonged light illumination over 60 s was strictly limited, provoking an osmotic ion diffusion against the photothermal ionic flux (Figure S4). The resulting ionic Seebeck coefficient is in the range of 0.6 to $0.9 \text{ mV}\cdot\text{K}^{-1}$ while revealing thermal enhancement. It is worth mentioning that a photoinduced charge separation can also impact the mobile-ion flux through fluidic nanochannels according to recent studies.^{44–47} Particularly, in nanochannels associated with wide band gap semiconducting materials, a concomitantly created trans-membrane potential by the charge separation can induce a directional and charge-selective ionic flow across the channel.

To understand the effects of photoelectronic responses of conduits on the permeating ionic flux, a Nb_2CT_x MXene showing a different thermoelectric feature is comparatively investigated (Figure S5). The Nb_2CT_x membranes exhibit an identical lamellar configuration to $\text{Ti}_3\text{C}_2\text{T}_x$ membranes, and the highly ordered interlayer spacing was confirmed from the fully hydrated membranes. Furthermore, the Nb_2CT_x membranes demonstrate comparable optical absorptivity to that of $\text{Ti}_3\text{C}_2\text{T}_x$. Static thermoelectric measurement of both $\text{Ti}_3\text{C}_2\text{T}_x$ and Nb_2CT_x reveals their contrasting response under a temperature gradient (Figure S6). Given that the $\text{Ti}_3\text{C}_2\text{T}_x$ MXene behaves as a metal-like conductor,⁴⁸ such an opposite response from the Nb_2CT_x membrane suggests the dominant presence of a hole charge carrier. The majority carrier in the Nb_2CT_x sheets could be reconfirmed by Hall effect measurements as well as Seebeck coefficient measurements. However, under light illumination, the Nb_2CT_x channel shows no discrepancy in magnitude and polarity of the ionic Seebeck coefficient compared to those of $\text{Ti}_3\text{C}_2\text{T}_x$ membranes (Figure S7). Furthermore, both species $\text{Ti}_3\text{C}_2\text{T}_x$ and Nb_2CT_x exhibit the same directional flux of cations even under a direct joule-

heating-induced temperature gradient (Figure S8). Hence, we postulate that the photothermal ion transport is dominantly governed by the temperature-gradient-derived chemical potential across the MXene fluidic channels.

More interestingly, the charge selectivity of the ion channels can play a central role in regulation of trans-nanochannel photothermal potential (ϕ_m) under a temperature difference, according to previously suggested nonisothermal ion transport models as^{11,29}

$$\phi_m = \frac{(2t_+ - 1)R}{F}(T_1 \ln c_1 - T_2 \ln c_2)$$

where R is the gas constant, F is the Faraday constant, and T_i and c_i are, respectively, the temperature and the salt concentration at designated reservoirs. To experimentally discern the relationship between cation permselectivity and ionic Seebeck coefficient, we explored the photothermal voltages at various KCl concentrations and under regulated pH. The intensity of irradiated light is fixed to $100 \text{ mW}\cdot\text{cm}^{-2}$ while maintaining equimolar concentrations between two electrolyte reservoirs. With decreasing salinity, the ionic Seebeck coefficient obviously exhibits an incremental performance, reaching $1.0 \text{ mV}\cdot\text{K}^{-1}$ at a concentration of $10^{-4} \text{ mol}\cdot\text{L}^{-1}$ (Figure 4a). The Seebeck coefficient, which is inversely proportional to the concentration, can be understood as a consequence of enhanced charge selectivity at lower concentration, as proven earlier. This salinity-related thermoelectric response is previously reported from commercially available cation exchange membranes (Figure S9).⁴¹ Note that the narrow interplanar channels can exert a compression effect or dehydration on the potassium ions having a similar hydration shell size with the effective channel height.^{15,49,50} This implies that for larger cations than a nanochannel, the steric effect with increased hydrated sizes can limit the cationic permeation through the nanochannels, producing lower photothermal voltages. Meanwhile, at an acidic condition of pH 3.34, the suppressed photothermal voltage was observed (Figure S10). When the pH is decreased, the protonation of the terminal groups on MXene sheets leads to reduced negative surface charges, accumulating less counterions on their interplanar spacing.^{14,51} The fewer cations inside channels and the associated decrease of cationic selectivity consequentially yield a lower ionic Seebeck coefficient.

The ionic photothermal response is further investigated in the presence of a salt concentration gradient as shown in Figure 4b and c. When the light is irradiated on the membrane near the diluted side, the thermo-osmotic ionic flux from cold

to hot is aligned to the direction of self-diffusive ion flux, as shown in the inset. The ionic Seebeck coefficient from the interpolated output voltages is estimated to be $0.81 \text{ mV}\cdot\text{K}^{-1}$. The observed higher ionic Seebeck coefficient under a salt gradient, taking the applied higher concentration into account, is most likely due to the self-diffusion-driven, lowered energy barrier for cation passage.⁵² Additionally, the photothermoelectric response was stable and reproducible on a 1000 s time scale. For practical purposes, we devised a photothermosensitive system with a large-area transmembrane in contact with an ionic gel electrolyte (Figure S11). Under light illumination, a stable heat transfer through a quasi-solid-state gel creates a stable temperature gradient across the membrane. The device, despite a limited temperature change across the membranes, obviously displays a light intensity-sensitive response as well as reproducible thermal voltages.

CONCLUSION

In summary, we have employed subnanometer confined ion conductors in lamellar $\text{Ti}_3\text{C}_2\text{T}_x$ MXene membranes as a bionic thermosensitive platform. The nanoconfined channels covered by an electrical double layer lead to highly charge-selective ion diffusion under the electrochemical potential. Coupled with the inherent photothermal properties of MXenes, the cation-selective transport by localized photothermal stimuli is converted to a trans-nanochannel diffusion potential, corresponding to open-circuit voltage over a temperature gradient. A thermoelectric response of up to $1.0 \text{ mV}\cdot\text{K}^{-1}$ was obtained under one sun illumination, comparable to that of biological thermosensory channels. Such photothermoelectric responses show not only obvious dependency on the cationic permselectivity of nanochannels, as anticipated from the theoretical consideration, but also its high sensitivity even under a tiny thermal gradient of $<1 \text{ K}$. Moreover, the MXene channels exhibited stable and reproducible response in the absence and presence of an ionic concentration gradient. Our work advances a fundamental understanding of the photothermo-osmotic ion transport in MXene, providing an avenue for the application of MXene membranes in biomimetic sensory systems.

EXPERIMENTAL SECTION

Fabrication of MXene Lamellar Membranes. $\text{Ti}_3\text{C}_2\text{T}_x$ and Nb_2CT_x MXene were synthesized as previously reported in our work.⁵³ Specifically, the MAX phase Ti_3AlC_2 etchant was prepared by the method in which 1 g of lithium fluoride (LiF 98%, Alfa Aesar) was slowly added into 20 mL of $9 \text{ mol}\cdot\text{L}^{-1}$ hydrochloric (HCl 35–38%, Fisher Scientific) and stirred at 500 rpm for 5 min. All chemicals were used as received without further purification. The 1 g of Ti_3AlC_2 powder (98 wt %, 400 mesh, Laizhou Kai Kai Ceramic Materials Co., Ltd.) was immersed in the as-prepared etching solution at $40 \text{ }^\circ\text{C}$ for 24 h. The slurry was centrifuged and rinsed several times using deionized water until the pH of the supernatant was around 6. Then, the sediment was intercalated by 10 mL of $1 \text{ mol}\cdot\text{L}^{-1}$ tetramethylammonium hydroxide (TMAOH) at room temperature for 24 h and centrifuged three times at 11 000 rpm for 10 min. After intercalation, the dark green $\text{Ti}_3\text{C}_2\text{T}_x$ MXene suspension can be collected after 5 min of centrifugation at 3500 rpm using deionized water. The experimental procedure for the synthesis of Nb_2CT_x MXene is the same as above, except that the raw material Nb_2AlC was etched by 20 mL of 49% hydrofluoric acid. The lamellar MXene membranes were fabricated by filtering specific amounts of an MXene dispersion through a polyvinylidene fluoride (PVDF) membrane (0.22 μm pore size and a diameter of 43 mm). All filtrated membranes

were ambient-dried overnight and could be easily detached from the support.

Ion Transport Measurements. The fluidic cell fabricated with a polydimethylsiloxane elastomer was custom-made for the ion transport measurement. The MXene lamellar membranes trimmed into rectangular pieces were embedded in the PDMS prepolymer and curing agent, and after curing the elastomer, two electrolyte reservoirs were carved out to expose two ends of the PDMS-immersed MXene membranes to the electrolyte solution. The MXene nanofluidic devices were then immersed in electrolytes for at least 1 day for fully hydrating the fluidic channels. The ionic transport measurement was performed by taking the current–voltage characteristics across the trans-nanochannels at room temperature, using a Keithley 2400 sourcemeter. The measurements were performed at various KCl concentrations of 10^{-4} to $1 \text{ mol}\cdot\text{L}^{-1}$. A pair of Ag/AgCl electrodes was employed to measure the ionic transport across membranes. For specific measurement under the concentration gradient, a pair of commercial salt-bridge electrodes (CHI111P, CH Instruments, Inc.) was applied. The Ag/AgCl electrodes in $1 \text{ mol}\cdot\text{L}^{-1}$ KCl that contact the electrolyte reservoir *via* porous Teflon salt bridges can eliminate the potential generated from the redox reaction on the electrodes under unequal ionic strength.^{19,54} For the photothermal reaction, the MXene membranes were irradiated with a Newport 94043A solar simulator with an optical filter for the standard AM 1.5G spectrum, and resulting temperature changes over the MXene membranes were captured by an infrared camera (A600-series, FLIR). Under localized light illumination, the open-circuit voltages corresponding to photothermoelectric ionic voltages were measured across the MXene nanochannels. The thermoelectric ion transport was further investigated using localized Joule heating over the MXene nanofluidic devices. Carbon nanotube–poly(vinyl alcohol) composite films were applied as a Joule heater electrically connected with a DC power supply.⁵⁵

Solid-State Thermoelectric Transport Measurement. The static thermoelectric transports of $\text{Ti}_3\text{C}_2\text{T}_x$ and Nb_2CT_x are comparatively studied using a closed circuit wherein the MXene membrane is serially connected with the Keithley 2400 sourcemeter. Temperature control over the MXene channels was carried out by using a commercial thermoelectric generator module. Under local heating or cooling, the thermoelectric current by diffusion of thermally activated majority carriers was measured across the MXene membranes. More precisely, the Seebeck coefficient of the free-standing MXene films ($1 \times 1 \text{ cm}^2$) was tested in the in-plane direction by a commercial thermoelectric measurement system (RZ200Li, Ozawa Science Co. Ltd.). During the measurement, a dynamic flow of 4% H_2/Ar was supplied to obtain a reducing surrounding. The conductivity was measured by the four-probe method under thermal equilibrium in each temperature. Hereafter, a small temperature difference along the sample channel was created by local cooling at one side of the sample. Two inner probes are also the Pt thermometers; therefore, the Seebeck voltage (ΔV) and the temperature gradient (ΔT) could be measured simultaneously. According to the formula $S = \Delta V/\Delta T$, the Seebeck coefficient could be obtained. In each temperature, five different data points were collected and analyzed. The details were shown in our previous work.⁵⁶

Hall Effect Measurement. Carrier concentration and Hall mobility of the MXene membranes were measured by a Hall-effect measurement system (7700A, Lake Shore) using the van der Pauw technique for $1 \times 1 \text{ cm}^2$ samples at RT under a magnetic field range of ± 5 to $\pm 20 \text{ KG}$ by linear sweep with field reversal mode. Ohmic contact was achieved by fast-drying silver paste (Ted Pella) at the four corners of the sample with lead wires from a printed circuit board for the measurement.

Characterizations. A field emission scanning electron microscope (Merlin, Carl Zeiss) was used to characterize the microstructures of the MXene lamellar membranes. The XRD analysis was conducted by using Bruker D8 Advance with $\text{Cu K}\alpha$ radiation ($\lambda = 0.15406 \text{ nm}$); the step scan was 0.02° over a step time of 2 s. The diffuse reflectance from 200 to 800 nm wavelength was measured using ultraviolet visible

absorption spectroscopy (Cary 5000, Agilent). The zeta potential of the MXene suspension was measured over a range of pH with a Malvern Zetasizer Nano ZS.

ASSOCIATED CONTENT

Supporting Information

The Supporting Information is available free of charge at <https://pubs.acs.org/doi/10.1021/acsnano.0c04099>.

Morphologies of the exfoliated $Ti_3C_2T_x$ MXene sheets, determination of nanochannel dimensions in lamellar MXene membranes, photothermal response of the MXene cation channels, effect of prolonged light irradiation on the photothermal voltage generation, Nb_2CT_x MXene-guided ion channels, solid-state thermoelectric transport of $Ti_3C_2T_x$ and Nb_2CT_x MXene membranes, photothermal response of Nb_2CT_x MXene membranes, ionic transport under Joule-heating-driven temperature gradient, comparative study with commercially available cation exchange membranes, photothermal voltage generation at lower pH, photothermo-sensing device (PDF)

AUTHOR INFORMATION

Corresponding Authors

Peng Wang – Water Desalination and Reuse Center, Division of Biological and Environmental Science and Engineering, King Abdullah University of Science and Technology, Thuwal 23955-6900, Saudi Arabia; Department of Civil and Environmental Engineering, The Hong Kong Polytechnic University, Kowloon, Hong Kong; orcid.org/0000-0003-0856-0865; Email: peng.wang@kaust.edu.sa

Husam N. Alshareef – Materials Science and Engineering, Physical Sciences and Engineering Division, King Abdullah University of Science and Technology, Thuwal 23955-6900, Saudi Arabia; orcid.org/0000-0001-5029-2142; Email: husam.alshareef@kaust.edu.sa

Authors

Seunghyun Hong – Materials Science and Engineering, Physical Sciences and Engineering Division and Water Desalination and Reuse Center, Division of Biological and Environmental Science and Engineering, King Abdullah University of Science and Technology, Thuwal 23955-6900, Saudi Arabia; orcid.org/0000-0001-5810-9250

Guodong Zou – Materials Science and Engineering, Physical Sciences and Engineering Division, King Abdullah University of Science and Technology, Thuwal 23955-6900, Saudi Arabia

Hyunho Kim – Materials Science and Engineering, Physical Sciences and Engineering Division, King Abdullah University of Science and Technology, Thuwal 23955-6900, Saudi Arabia; orcid.org/0000-0003-2381-9716

Dazhen Huang – Materials Science and Engineering, Physical Sciences and Engineering Division, King Abdullah University of Science and Technology, Thuwal 23955-6900, Saudi Arabia

Complete contact information is available at: <https://pubs.acs.org/doi/10.1021/acsnano.0c04099>

Notes

The authors declare no competing financial interest.

ACKNOWLEDGMENTS

Research reported in this work was supported by King Abdullah University of Science and Technology (KAUST).

REFERENCES

- (1) de la Escosura-Muñiz, A.; Merkoçi, A. Nanochannels Preparation and Application in Biosensing. *ACS Nano* **2012**, *6*, 7556–7583.
- (2) Martin, C. R.; Siwy, Z. S. Learning Nature's Way: Biosensing with Synthetic Nanopores. *Science* **2007**, *317*, 331–332.
- (3) Vriens, J.; Nilius, B.; Voets, T. Peripheral Thermosensation in Mammals. *Nat. Rev. Neurosci.* **2014**, *15*, 573–589.
- (4) Castillo, K.; Diaz-Franulic, I.; Canan, J.; Gonzalez-Nilo, F.; Latorre, R. Thermally Activated TRP Channels: Molecular Sensors for Temperature Detection. *Phys. Biol.* **2018**, *15*, 021001.
- (5) Reber, N.; Küchel, A.; Spohr, R.; Wolf, A.; Yoshida, M. Transport Properties of Thermo-Responsive Ion Track Membranes. *J. Membr. Sci.* **2001**, *193*, 49–58.
- (6) Jung, Y.; Bayley, H.; Movileanu, L. Temperature-Responsive Protein Pores. *J. Am. Chem. Soc.* **2006**, *128*, 15332–15340.
- (7) Yameen, B.; Ali, M.; Neumann, R.; Ensinger, W.; Knoll, W.; Azzaroni, O. Ionic Transport through Single Solid-State Nanopores Controlled with Thermally Nanoactuated Macromolecular Gates. *Small* **2009**, *5*, 1287–1291.
- (8) Guo, W.; Xia, H.; Xia, F.; Hou, X.; Cao, L.; Wang, L.; Xue, J.; Zhang, G.; Song, Y.; Zhu, D.; Wang, Y.; Jiang, L. Current Rectification in Temperature-Responsive Single Nanopores. *ChemPhysChem* **2010**, *11*, 859–864.
- (9) Zhang, Z.; Xie, G.; Xiao, K.; Kong, X.-Y.; Li, P.; Tian, Y.; Wen, L.; Jiang, L. Asymmetric Multifunctional Heterogeneous Membranes for pH- and Temperature-Cooperative Smart Ion Transport Modulation. *Adv. Mater.* **2016**, *28*, 9613–9619.
- (10) Zhou, Y.; Guo, W.; Cheng, J.; Liu, Y.; Li, J.; Jiang, L. High-Temperature Gating of Solid-State Nanopores with Thermo-Responsive Macromolecular Nanoactuators in Ionic Liquids. *Adv. Mater.* **2012**, *24*, 962–967.
- (11) Chen, K.; Yao, L.; Su, B. Bionic Thermoelectric Response with Nanochannels. *J. Am. Chem. Soc.* **2019**, *141*, 8608–8615.
- (12) Hwang, J.; Sekimoto, T.; Hsu, W.-L.; Kataoka, S.; Endo, A.; Daiguji, H. Thermal Dependence of Nanofluidic Energy Conversion by Reverse Electrodialysis. *Nanoscale* **2017**, *9*, 12068–12076.
- (13) Xie, G.; Li, P.; Zhang, Z.; Xiao, K.; Kong, X.-Y.; Wen, L.; Jiang, L. Skin-Inspired Low-Grade Heat Energy Harvesting Using Directed Ionic Flow through Conical Nanochannels. *Adv. Energy Mater.* **2018**, *8*, 1800459.
- (14) Hong, S.; Ming, F.; Shi, Y.; Li, R.; Kim, I. S.; Tang, C. Y.; Alshareef, H. N.; Wang, P. Two-Dimensional $Ti_3C_2T_x$ MXene Membranes as Nanofluidic Osmotic Power Generators. *ACS Nano* **2019**, *13*, 8917–8925.
- (15) Hong, S.; Constans, C.; Surmani Martins, M. V.; Seow, Y. C.; Guevara Carrió, J. A.; Garaj, S. Scalable Graphene-Based Membranes for Ionic Sieving with Ultrahigh Charge Selectivity. *Nano Lett.* **2017**, *17*, 728–732.
- (16) Bocquet, L.; Charlaix, E. Nanofluidics, from Bulk to Interfaces. *Chem. Soc. Rev.* **2010**, *39*, 1073–1095.
- (17) Schoch, R. B.; Han, J.; Renaud, P. Transport Phenomena in Nanofluidics. *Rev. Mod. Phys.* **2008**, *80*, 839–883.
- (18) Nair, R. R.; Wu, H. A.; Jayaram, P. N.; Grigorieva, I. V.; Geim, A. K. Unimpeded Permeation of Water through Helium-Leak-Tight Graphene-Based Membranes. *Science* **2012**, *335*, 442–444.
- (19) Rollings, R. C.; Kuan, A. T.; Golovchenko, J. A. Ion Selectivity of Graphene Nanopores. *Nat. Commun.* **2016**, *7*, 11408.
- (20) Feng, J.; Graf, M.; Liu, K.; Ovchinnikov, D.; Dumcenco, D.; Heiraniyan, M.; Nandigana, V.; Aluru, N. R.; Kis, A.; Radenovic, A. Single-Layer MoS_2 Nanopores as Nanopower Generators. *Nature* **2016**, *536*, 197–200.
- (21) Siria, A.; Poncharal, P.; Bianco, A.-L.; Fulcrand, R.; Blase, X.; Purcell, S. T.; Bocquet, L. Giant Osmotic Energy Conversion

Measured in a Single Transmembrane Boron Nitride Nanotube. *Nature* **2013**, *494*, 455–458.

(22) Anasori, B.; Lukatskaya, M. R.; Gogotsi, Y. 2D Metal Carbides and Nitrides (MXenes) for Energy Storage. *Nat. Rev. Mater.* **2017**, *2*, 16098.

(23) Anasori, B.; Gogotsi, Y. Introduction to 2D Transition Metal Carbides and Nitrides (MXene). In *2D Metal Carbides and Nitrides (MXenes) Structure, Properties and Applications Structure, Properties and Applications*; Anasori, B., Gogotsi, Y., Eds.; Springer: Berlin, 2019; pp 3–12.

(24) Ding, L.; Xiao, D.; Lu, Z.; Deng, J.; Wei, Y.; Caro, J.; Wang, H. Oppositely Charged $Ti_3C_2T_x$ MXene Membranes with 2D Nanofluidic Channels for Osmotic Energy Harvesting. *Angew. Chem., Int. Ed.* **2020**, *59*, 8720–8726.

(25) Ding, L.; Li, L.; Liu, Y.; Wu, Y.; Lu, Z.; Deng, J.; Wei, Y.; Caro, J.; Wang, H. Effective Ion Sieving with $Ti_3C_2T_x$ MXene Membranes for Production of Drinking Water from Seawater. *Nat. Sustain.* **2020**, *3*, 296–302.

(26) Lu, Z.; Wei, Y.; Deng, J.; Ding, L.; Li, Z.-K.; Wang, H. Self-Crosslinked MXene ($Ti_3C_2T_x$) Membranes with Good Antiswelling Property for Monovalent Metal Ion Exclusion. *ACS Nano* **2019**, *13*, 10535–10544.

(27) Li, R.; Zhang, L.; Shi, L.; Wang, P. MXene Ti_3C_2 : An Effective 2D Light-To-Heat Conversion Material. *ACS Nano* **2017**, *11*, 3752–3759.

(28) Szuplewska, A.; Kulpińska, D.; Dybko, A.; Jastrzębska, A. M.; Wojciechowski, T.; Rozmysłowska, A.; Chudy, M.; Grabowska-Jadach, I.; Ziemkowska, W.; Brzózka, Z.; Olszyna, A. 2D Ti_2C (MXene) as a Novel Highly Efficient and Selective Agent for Photothermal Therapy. *Mater. Sci. Eng., C* **2019**, *98*, 874–886.

(29) Barragán, V. M.; Kjelstrup, S. Thermo-Osmosis in Membrane Systems: A Review. *J. Non-Equilib. Thermodyn.* **2017**, *42*, 217–236.

(30) Ghidui, M.; Lukatskaya, M. R.; Zhao, M.-Q.; Gogotsi, Y.; Barsoum, M. W. Conductive Two-Dimensional Titanium Carbide ‘Clay’ with High Volumetric Capacitance. *Nature* **2014**, *516*, 78–81.

(31) Wang, X.; Shen, X.; Gao, Y.; Wang, Z.; Yu, R.; Chen, L. Atomic-Scale Recognition of Surface Structure and Intercalation Mechanism of Ti_3C_2X . *J. Am. Chem. Soc.* **2015**, *137*, 2715–2721.

(32) Wang, J.; Chen, P.; Shi, B.; Guo, W.; Jaroniec, M.; Qiao, S.-Z. A Regularly Channeled Lamellar Membrane for Unparalleled Water and Organics Permeation. *Angew. Chem., Int. Ed.* **2018**, *57*, 6814–6818.

(33) Ding, L.; Wei, Y.; Li, L.; Zhang, T.; Wang, H.; Xue, J.; Ding, L.-X.; Wang, S.; Caro, J.; Gogotsi, Y. MXene Molecular Sieving Membranes for Highly Efficient Gas Separation. *Nat. Commun.* **2018**, *9*, 155.

(34) Shen, J.; Liu, G.; Ji, Y.; Liu, Q.; Cheng, L.; Guan, K.; Zhang, M.; Liu, G.; Xiong, J.; Yang, J.; Jin, W. 2D MXene Nanofilms with Tunable Gas Transport Channels. *Adv. Funct. Mater.* **2018**, *28*, 1801511.

(35) Abraham, J.; Vasu, K. S.; Williams, C. D.; Gopinadhan, K.; Su, Y.; Cherian, C. T.; Dix, J.; Prestat, E.; Haigh, S. J.; Grigorieva, I. V.; Carbone, P.; Geim, A. K.; Nair, R. R. Tunable Sieving of Ions Using Graphene Oxide Membranes. *Nat. Nanotechnol.* **2017**, *12*, 546–550.

(36) Israelachvili, J. N. Interactions Involving Polar Molecules. In *Intermolecular and Surface Forces*, 3rd ed.; Academic Press: San Diego, 2011; pp 71–90.

(37) Lekner, J.; Dorf, M. C. Why Some Things Are Darker When Wet. *Appl. Opt.* **1988**, *27*, 1278–1280.

(38) Smeets, R. M. M.; Keyser, U. F.; Krapf, D.; Wu, M.-Y.; Dekker, N. H.; Dekker, C. Salt Dependence of Ion Transport and DNA Translocation through Solid-State Nanopores. *Nano Lett.* **2006**, *6*, 89–95.

(39) van der Heyden, F. H. J.; Stein, D.; Dekker, C. Streaming Currents in a Single Nanofluidic Channel. *Phys. Rev. Lett.* **2005**, *95*, 116104.

(40) Kim, D.-K.; Duan, C.; Chen, Y.-F.; Majumdar, A. Power Generation from Concentration Gradient by Reverse Electrodialysis in Ion-Selective Nanochannels. *Microfluid. Nanofluid.* **2010**, *9*, 1215–1224.

(41) Barragán, V. M.; Kristiansen, K. R.; Kjelstrup, S. Perspectives on Thermoelectric Energy Conversion in Ion-Exchange Membranes. *Entropy* **2018**, *20*, 905.

(42) Lao, J.; Wu, S.; Gao, J.; Dong, A.; Li, G.; Luo, J. Electricity Generation Based on a Photothermally Driven $Ti_3C_2T_x$ MXene Nanofluidic Water Pump. *Nano Energy* **2020**, *70*, 104481.

(43) Lao, J.; Lv, R.; Gao, J.; Wang, A.; Wu, J.; Luo, J. Aqueous Stable Ti_3C_2 MXene Membrane with Fast and Photoswitchable Nanofluidic Transport. *ACS Nano* **2018**, *12*, 12464–12471.

(44) Xiao, K.; Tu, B.; Chen, L.; Heil, T.; Wen, L.; Jiang, L.; Antonietti, M. Photo-Driven Ion Transport for a Photodetector Based on an Asymmetric Carbon Nitride Nanotube Membrane. *Angew. Chem., Int. Ed.* **2019**, *58*, 12574–12579.

(45) Xiao, K.; Chen, L.; Chen, R.; Heil, T.; Lemus, S. D. C.; Fan, F.; Wen, L.; Jiang, L.; Antonietti, M. Artificial Light-Driven Ion Pump for Photoelectric Energy Conversion. *Nat. Commun.* **2019**, *10*, 74.

(46) Yang, J.; Hu, X.; Kong, X.; Jia, P.; Ji, D.; Quan, D.; Wang, L.; Wen, Q.; Lu, D.; Wu, J.; Jiang, L.; Guo, W. Photo-Induced Ultrafast Active Ion Transport through Graphene Oxide Membranes. *Nat. Commun.* **2019**, *10*, 1171.

(47) Jia, P.; Wen, Q.; Liu, D.; Zhou, M.; Jin, X.; Ding, L.; Dong, H.; Lu, D.; Jiang, L.; Guo, W. Highly Efficient Ionic Photocurrent Generation through WS_2 -Based 2D Nanofluidic Channels. *Small* **2019**, *15*, 1905355.

(48) Kim, H.; Wang, Z.; Alshareef, H. N. MXetronics: Electronic and Photonic Applications of MXenes. *Nano Energy* **2019**, *60*, 179–197.

(49) Sint, K.; Wang, B.; Král, P. Selective Ion Passage Through Functionalized Graphene Nanopores. *J. Am. Chem. Soc.* **2008**, *130*, 16448–16449.

(50) Zwolak, M.; Lagerqvist, J.; Di Ventra, M. Quantized Ionic Conductance in Nanopores. *Phys. Rev. Lett.* **2009**, *103*, 128102.

(51) Natu, V.; Sokol, M.; Verger, L.; Barsoum, M. W. Effect of Edge Charges on Stability and Aggregation of $Ti_3C_2T_x$ MXene Colloidal Suspensions. *J. Phys. Chem. C* **2018**, *122*, 27745–27753.

(52) Gao, J.; Liu, X.; Jiang, Y.; Ding, L.; Jiang, L.; Guo, W. Understanding the Giant Gap between Single-Pore- and Membrane-Based Nanofluidic Osmotic Power Generators. *Small* **2019**, *15*, 1804279.

(53) Velusamy, D. B.; El-Demellawi, J. K.; El-Zohry, A. M.; Giugni, A.; Lopatin, S.; Hedhili, M. N.; Mansour, A. E.; Fabrizio, E. D.; Mohammed, O. F.; Alshareef, H. N. MXenes for Plasmonic Photodetection. *Adv. Mater.* **2019**, *31*, 1807658.

(54) Bard, A. J.; Faulkner, L. R. Potentials and Thermodynamics of Cells. In *Electrochemical Methods: Fundamentals and Applications*, 2nd ed.; Wiley: New York, 2000; pp 44–86.

(55) Dongare, P. D.; Alabastri, A.; Pedersen, S.; Zodrow, K. R.; Hogan, N. J.; Neumann, O.; Wu, J.; Wang, T.; Deshmukh, A.; Elimelech, M.; Li, Q.; Nordlander, P.; Halas, N. J. Nanophotonics-Enabled Solar Membrane Distillation for Off-Grid Water Purification. *Proc. Natl. Acad. Sci. U. S. A.* **2017**, *114*, 6936–6941.

(56) Kim, H.; Anasori, B.; Gogotsi, Y.; Alshareef, H. N. Thermoelectric Properties of Two-Dimensional Molybdenum-Based MXenes. *Chem. Mater.* **2017**, *29*, 6472–6479.